Electromechanical Modeling and Simulation of MEMS-Based Piezoelectric Vibration Energy Harvesting Device Using PZT-5H Material

Tuan Ngoc Dao, Phuoc Thanh Quang Le, Tho Quang Than, Son Thanh Nguyen, Tung Thanh Huynh, Phuoc-Anh Le, Phuc Hong Than*, Cong-Kha Pham

Abstract—In this study, we describe the operation of piezoelectric energy converters and electromechanical modeling of piezoelectric energy harvesting (PEH) devices based on microelectromechanical systems (MEMS) for low-power sensors. Consideration is given to a piezoelectric energy harvester based on standard MEMS. The parameters are determined and optimized using a simple MEMS cantilever model. On top of a Brass substrate, the model uses a single layer of piezoelectric material. We utilized the finite element method (FEM) models created with software tools NanoHUB and COMSOL to analyze the electromechanical behavior of MEMS-based piezoelectric energy harvesting (PEH) devices. The electromechanical modeling was applied to predict the modal and harmonic response of the PEH devices. By using a modal analysis, the resonant frequencies are 182 Hz for the FEM models of the PZT-5H PEH device through NanoHUB and COMSOL. The simulated MEMS can provide a voltage between 1.7 and 1.9 mV, 0.074 μW of output power. The produced voltage and output power may be increased by connecting the piezoelectric layers in parallel and series. And the Internet of Things (IoT) sensors might be driven by this array of devices.

Index Terms—Piezoelectric, MEMS, energy Harvesting, piezoelectric materials, finite element analysis.

1. Introduction

Recently, energy harvesting technology has been increased due to the development of IoT and the reduction in power consumption of electronic components such as wireless sensor nodes. A major limitation of IoT sensor nodes is the lifetime of batteries. Energy harvesting has been proposed as a self-power supply for these sensor nodes. There are many different ways to generate usable power, including through human activities, mechanical devices, vehicles, and even environmental energy sources, including solar, thermal, and radio frequency energy. Among environmental energy, vibration energy harvesters can convert vibration energy into electric energy, classified in two types; resonance and non-resonance type. Random vibration such as human movement is the non-resonance type, ambient vibration such as vehicle engine, 3-axis machine tool, railway is resonance type. The demand for self-powered autonomous devices will increase in the period when a lot of IoT sensors are produced and used in various places. Small vibration energy harvesters can be used as the power source of IoT sensor nodes which are installed at a variety of areas. Among vibration energy harvesters, many research efforts have been focused on piezoelectric vibration energy harvesters (pVEHs), energy harvesters with a simple-cantilerver structure, high mechanical quality factor, high output power, easy fabrication and and compatibility with micro-fabrication technology high output power [1]–[12]. Due to its high power density, simplicity of construction, and compatibility with microfabrication technology, piezoelectric energy harvesting concentrates on transferring mechanical vibration energy to electrical energy. Due to their capacity to resonate at low frequencies and produce more power, the majority of piezoelectric energy harvesters take the form of cantilevers. In this paper, we present the successful design and modeling of a piezoelectric vibration energy harvester based on the results of simulations performed in COMSOL Multiphysics and NanoHUB.

Tuan Ngoc Dao and Phuoc Thanh Quang Le are with The University of Danang - Vietnam Korea University of Information and Communication Technology, Danang, Vietnam.

Tho Quang Than is with Central Power Corporation (EVNCPC), Danang, Vietnam.

Son Thanh Nguyen is with National Institute of Technology, Kushiro College, Japan.

Tung Thanh Huynh is with The University of Danang - University of Science and Technology, Danang, Vietnam.

Phuoc-Anh Le is with College of Engineering and Computer Science, VinUniversity, Hanoi 100000, Vietnam.

Phuc Hong Than is with Duy Tan University (DTU), 3 Quang Trung, Hai Chau Dist., Danang, Vietnam.

Cong-Kha Pham is with The University of Electro-Communications (UEC), Tokyo, Japan.

**Corresponding author: Phuc Hong Than (e-mail: thanhongphuc@duytan.edu.vn)*

Manuscript received August 08, 2022; revised February 12, 2023; accepted March 15, 2023.
Digital Object Identifier 10.31130/ud-jst.2023.340ICT

2. Piezoelectric effect

2.1. Piezoelectric Effect

2.1.1. Working principle

The piezoelectric effect was first proposed by Pierre Curie and Jacques Curie in 1880. As illustrated in Fig. 1, crystals become electrically polarized when subjected to a mechanical force. This polarization generates a potential difference, which is inversely proportional to the applied force, through tension and compression. Conversely, when an electric field is applied to the crystal, this behavior is reversed. Depending on the intensity of the electric field, the crystal undergoes mechanical strain along the direction of the field. These phenomena are referred to as the inverse and direct piezoelectric effects, respectively. The forward and reverse piezo effects are normalized by the piezo components as follows [2]:

$$\begin{bmatrix} \delta \\ D \end{bmatrix} = \begin{bmatrix} s^E & d^t \\ d & \epsilon^T \end{bmatrix} \begin{bmatrix} \sigma \\ E \end{bmatrix} \tag{1}$$

Where δ and σ are the components strain and stress; D and E are the electric displacement and electric field components; s, ϵ, and d are elastic compliance, dielectric constant and piezoelectric coefficient, respectively. The symbols above E and T indicate that the respective constants are evaluated at constant electric field and constant stress, respectively; and the character above t stands for transpose. In practice, the direct piezoelectric effect is important for sensing and capturing energy when stress effects are used to generate charges on the surface of piezoelectric materials.

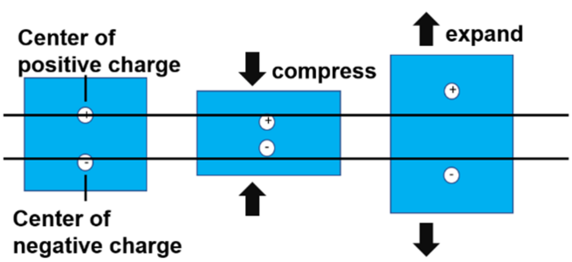

Fig. 1: The piezoelectric effect [2].

2.1.2. Piezoelectric material

The ability of piezoelectric materials to generate an electric charge under external stress or strain when an electric field is applied is a distinct property. Only 20 out of the 32-point groups of limited crystalline materials exhibit piezoelectricity, as illustrated in Fig. 2, based on their structural characteristics. Out of these 20 groups, the 10-point group is classified as t polar material, where an electric dipole moment occurs without any applied electric field. This is known as spontaneous polarization that changes with temperature, generating thermoelectricity.

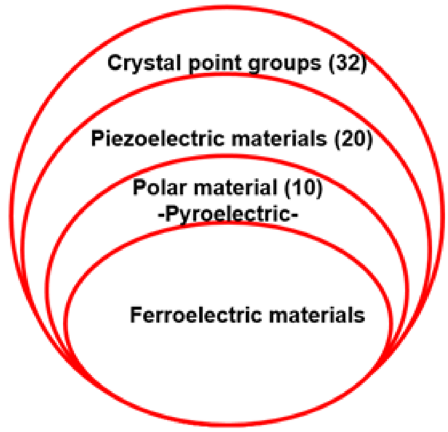

Fig. 2: Piezoelectric materials diagram [2].

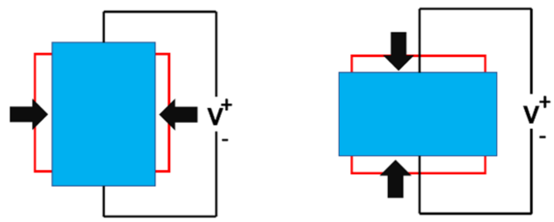

Fig. 3: Configuration of 33-mode and 31-mode [2].

2.1.3. Mode-31 and mode-33

A piezoelectric material has to be able to create both an electric charge and a potential difference when mechanical stress is applied in order for it to produce electrical energy. It is crucial to remember that the majority of piezoelectric materials used for energy harvesting have a particular polar axis (M), and the efficacy of energy harvesting will depend on the direction of the stress applied relative to this axis. The polarization direction determines the polar axis for ferroelectric ceramics or polymers. However, the crystallographic orientation along the c-axis of the Wurtzite crystal structure determines the polar axis for non-ferroelectric crystalline materials like AlN or ZnO. The "3" direction is seen as being on this polar axis. Due to symmetry, the other directions perpendicular to the polar axis are considered equivalent and referred to as the "1" direction. The applied stress can be either along the polar axis (direction 3) or perpendicular to it (direction 1), leading to two common piezoelectric energy harvesting configurations, known as mode 33 and mode 31, as depicted in Fig. 3. In mode 33, the stress/compression strain is applied parallel to axis 3, while the generated voltage is along the same axis. In mode 31, the stress strain is applied perpendicular to the polar axis and the generated voltage direction is at a right angle to the applied force. The piezoelectric coefficient (d_{3i}) is used to measure the efficiency of piezoelectric materials, which is defined as the ratio of open-circuit charge density to applied stress (in C/N).

The coefficient d_{33} is usually higher than the coefficient d_{31}. Mode 31 operation, on the other hand, results in a greater strain in direction 1 and is thus used in vibrating energy harvesting.

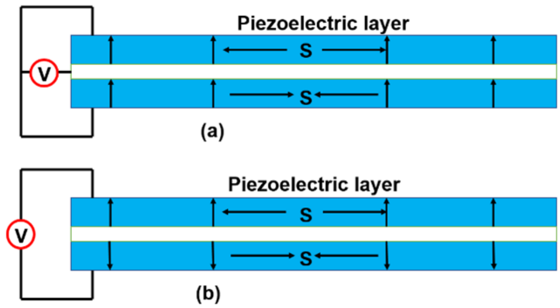

Fig. 4: (a) parallel polarized structure (b) series polarized structure [2].

2.2. Mechanical and electrical model

2.2.1. Model of a piezoelectrical harvester

Fig. 5 depicts a vibration-based energy harvester, which can be a sinusoidal mass-spring-damping mechanism (SDOF). The SDOF consists of a mass (M) suspended by a spring with a stiffness (K), damping constant (C), and resonant frequency. You may write the resonance frequency as:

$$\omega_n = \sqrt{K/M} \tag{2}$$

The mass movement is gradually reduced by mechanical damping (C_m) and electrical damping (C_e).

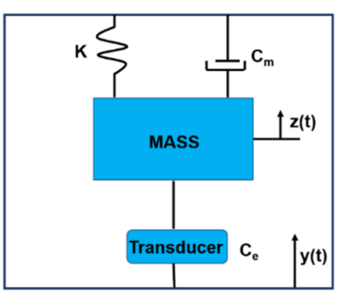

Fig. 5: Mode of a spring-based mass damping [2].

The inertial mass shifts out of phase with the system's bases when it is aroused by an external displacement, $y(t)$, and the resulting relative displacement is $z(t)$. The following may be used to represent the motion control equation for a damping system with a combined spring mass:

$$M\ddot{z}(t) + C\dot{z}(t) + Kz(t) = M\ddot{y}(t) \tag{3}$$

Equation (3) can also be written in terms of damped oscillation constants and natural frequencies. The damping factor ζ, including mechanical damping ζ_m and electrical damping ζ_e, (= ζ_m + ζ_e) is a dimensionless quantity defined as:

$$\zeta = \frac{c}{2m\omega_n} = C/2\sqrt{MK} \tag{4}$$

In the case of a beam, the stiffness K is given by $K = 3Y_c I/L^3$, Yc is Young's modulus, I is the moment of inertia and L is the length of the beam. The moment of inertia for the rectangular cross-section can be given as $I = (1/12)bh_3$, b and h being the beam's width and height, respectively. For cross-sectional areas and other stiffnesses, the formula can be found in the standard mechanical engineering manual [13], [14]. The ratio between relative displacement $z(t)$ (i.e. output) and external displacement $y(t)$ (i.e. input) can be obtained by applying the Laplace transform with zero initial condition in formula (2) is as follows [2]:

$$|\frac{Z(s)}{Y(s)}| = \frac{s^2}{s^2 + 2\zeta\omega_n s + \omega_n^2} \tag{5}$$

By assuming the external excitation $y(t) = Y_0 sin(\omega t)$, Y_0 and the excitation amplitude and frequency, respectively, the time domain $z(t)$ can be obtained by applying the above inverse Laplace transform (5), which is given as:

$$z(t) = \frac{Y_0(\omega/\omega_n)^2}{\sqrt{1-((\omega/\omega_n)^2)^2 + ((2\zeta\omega/\omega_n)^2)}} sin(\omega t - \phi) \tag{6}$$

Where $z(t)$ is the net shift $z(t) = Z_0 sin(\omega t - \phi)$, the phase angle between the output and the input can be expressed as:

$$\phi = arctan(\frac{C\omega}{K - M\omega^2}) \tag{7}$$

Fig. 6 displays an energy conversion diagram for an energy collecting system. From the input vibration energy U_{IN}, the spring mass damper system produces kinetic energy U_K and spring potential energy U_S. When mechanical and electrical dampers are present, kinetic energy (U_C) is dissipated from the system and converted to electrical energy (U_E) and loss energy (U_L).

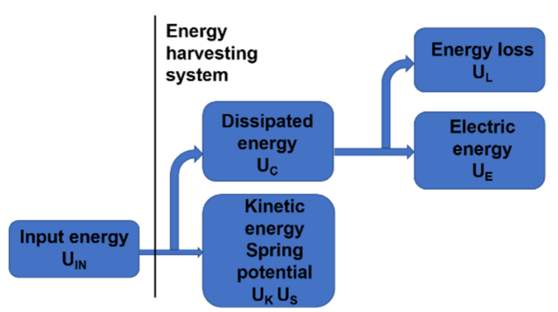

Fig. 6: Diagram of illustrated energy conversion diagram for an energy harvesting system [2].

The energy dissipated in each cycle U_C is simply the distance integral of the damping factor C_Z in one cycle:

$$U_c = 2C\int_{-Z_0}^{Z_0} \dot{z}dz \tag{8}$$

Integrating in (8) gives the magnitude Z_0 given by (6) and multiplying by the angular frequency gives the expression for the dissipated power:

$$P = \frac{m\zeta Y_0^2(\omega/\omega_n)^3\omega^3}{(1-(\omega/\omega_n)^2)^2 + (2\zeta\omega/\omega_n)^2} \tag{9}$$

Setting the operating frequency as the resonant frequency (ω = ω_n) in (9) yields the highest power:

$$P_{max} = \frac{mY_o^2\omega_n^3}{4\zeta} \tag{10}$$

From (10), it can be seen that when the energy receiver operates at a suitable frequency, the power generated can be maximized by reducing damping, increasing natural frequency, mass and excitation amplitude. In principle, zero damping will produce infinite power at resonance; however, in practice this is not possible. Reducing the damping coefficient will increase the displacement of the mass. The maximum available displacement of the mass Z_L is limited by the size and shape of the energy collector as shown in Fig. 9. Therefore, the damping factor must be large enough to prevent the mass from moving beyond the limit. The optimum value of the damping factor ζ_opt exists when the mass displacement falls just below the Z limit L and an unbiased resonance period is reached. Therefore, the limited optimal power is achieved by operating as close to ζ_opt as possible while observing the link displacement [15]–[24]. By rearranging (7), the optimal limiting damping factor ζ_opt is presented as [2]:

$$\zeta_{opt} = \frac{1}{2\omega_c}\sqrt{\omega_c^4(\frac{Y_0}{Z_L})^2 - (1-\omega_c^2)^2} \tag{11}$$

where ω_c is the ratio between the excitation frequency and the resonant frequency. By substituting (11) for (10), the maximum power wasted under the restricted mode of displacement condition may be found:

$$P_{Cmax} = \frac{mY_0^2\omega^3}{2\omega_c^2}(\frac{Z_l}{Y_0})^2\sqrt{\omega_c^4(\frac{Y_0}{Z_L})^2 - (1-\omega_c^2)^2} \tag{12}$$

Therefore, by setting $\omega_c = 1$ (i.e. $\omega = \omega_n$) at (12), the power wasted at resonance can be determined as:

$$P_{Cres} = \frac{1}{2}mY_0\omega_n^3 Z_L \tag{13}$$

Equation (13) gives the maximum power dissipated at resonance conditions for the limited mass displacement Z_L. Dissipated power can be converted into electrical power using piezoelectric, electromagnetic, and electrostatic mechanisms.

2.2.2. Equivalent circuit

Piezoelectric MEMS energy receivers with a block at the top have been the most studied and reported configuration. Fig. 7 shows a schematic design and equivalent circuit model of a piezoelectric beam with a single block positioned at the end of the beam.

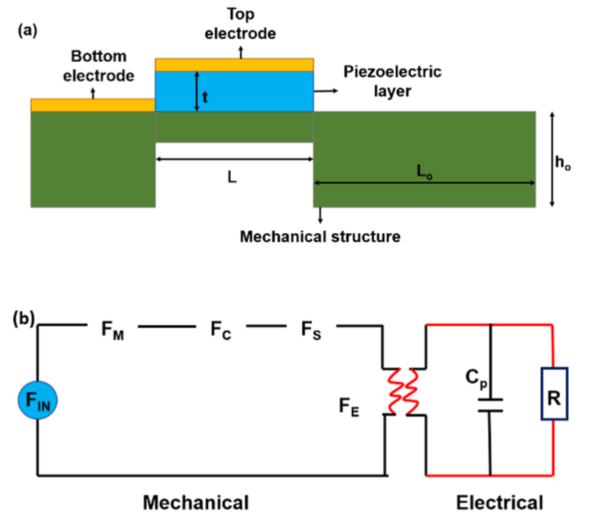

Fig. 7: (a) Schematic diagram (b) Equivalent circuit model of a traditional piezoelectric MEMS energy harvester [2].

The piezoelectric thin film on the beam is sandwiched between the bottom and top electrode layers. Fig. 7(b) depicts its equivalent circuit. The mass motion is coupled to the piezoelectric converter in the form of damped oscillations. Thus, the equation of the piezoelectric harvester can be obtained by applying Kirchhoff's law (KCL).

$$F_M + F_C + F_K + F_E = F_{IN} \tag{14}$$

Where F_{IN} denotes the overall force acting on the system, F_M denotes the mass's kinetic energy, F_C denotes the mechanical damping force, F_K denotes the spring's elastic potential energy, and F_E denotes the internal force brought on by the internal electric process voltage produced by piezoelectric materials. The electric displacement and strain inside the piezoelectric material of the microcantilever in mode 31 or mode 33 are given by component (1) as the following expressions [2]:

$$\delta = \frac{1}{Y_c}\sigma + d_{3i}E \tag{15}$$

$$D = d_{3i}\sigma + \epsilon_{3i}E \tag{16}$$

Where d_{3i} and ϵ_{3i} are piezoelectric coefficients and dielectric constants in mode 31 or 33. From (15), the stress caused by voltage generation of piezoelectric pieces is as follows [2]:

$$\sigma_e = d_{3i}Y_C E \tag{17}$$

From this, the mechanical internal and external forces of an equivalent circuit are defined by the equation [2]:

$$M\ddot{z} + C_m\dot{z} + Kz + \frac{c_1 Y_c d_{3i}}{g_e}v = -M\ddot{y} \tag{18}$$

Where v is the voltage across the load resistance and c_1 is the ratio of the binding force to the stress in the piezoelectric (i.e., $c_1 = F_E/\sigma_e$). The electric surface can be expressed using Kirchhoff's law [2].

$$\frac{c_2 d_{3i} g_e}{\epsilon_{3i}} \ddot{z} - \frac{1}{RC_p} v = \dot{v} \tag{19}$$

where c_2 is the ratio between the stress of the piezoelectric film and the vertical displacement of the block [16] (ie, $c_2 = z/\delta$). R is the load resistance and C_p is the total capacitance between the electrodes. For a mode 33 receiver with n pairs of IDEs, the total capacitance is the sum of each separate capacitance C_i.
Laplace transforms the (18) and (19), output voltage v can be expressed as [2]:

$$v = \frac{-j\omega \frac{c_2 d_{3i} g_e}{\epsilon_{3i}} \ddot{y}}{[\frac{1}{RC_p}\omega_n^2 - (\frac{1}{RC_p} + 2\zeta_m\omega_n)\omega^2] + j\omega[\omega_n^2(1+k_p^2) + \frac{2\zeta_m\omega_n}{RC_p} - \omega^2]} \tag{20}$$

$k_p^2 = Y_c d_{3i}^2/\epsilon_{3i}$ is the formula for the electromechanical coupling coefficient, or k_p. When the ambient oscillation's frequency coincides with the piezoelectric beam's resonance frequency (n = 1), (20) may be simplified as follows [2]:

$$v = \frac{-j\frac{c_2 d_{3i} g_e}{\epsilon_{3i}} \ddot{y}}{2\zeta_m\omega_n^2 + j(\omega_n^2 k_p^2 + \frac{2\zeta_m\omega_n}{RC_p})} \tag{21}$$

From there, the output power transmitted to the load will be described by the equation [2]:

$$P = \frac{1}{2} \frac{RC_p^2(\frac{c_2 d_{3i} g_e}{\epsilon_{3i}})^2}{(RC_p\omega_n)^2(4\zeta_m^2 + k_p^4) + RC_p 4\zeta_m\omega_n k_p^2 + 4\zeta_m^2} \frac{\ddot{y}^2}{\omega_n^2} \tag{22}$$

3. Piezoelectric beam simulation

To obtain the displacement of the end mass and the generated power as a function of excitation frequency, we conducted a simulation of the system. The simulation was performed within a frequency range of 1 to 200 Hz with an acceleration of 0.2 g. The data utilized to simulate a piezoelectric beam is presented in [25].

TABLE 1: Optimized structure parameters of the MEMS device.

Description	Values	Unit
Beam length	50	mm
Beam width	5	mm
Piezoelectric thickness	0.5	mm
Substrate thickness	0.5	mm
Mass length	1	mm
End-mass density	9000	kg/m³
Piezoelectric material	PZT-5H	
Substrade	Brass	

The output power of the MEMS is depicted in Fig. 8 as a function of piezoelectric material type. In the group of all piezoelectric materials shown in Fig. 8, the energy harvested by the MEMS component made of PZT-5H material is the highest, while that of the MEMS made of PZT-5A material is the lowest. Therefore, we have chosen PZT-5H as the piezolectric material for this study.

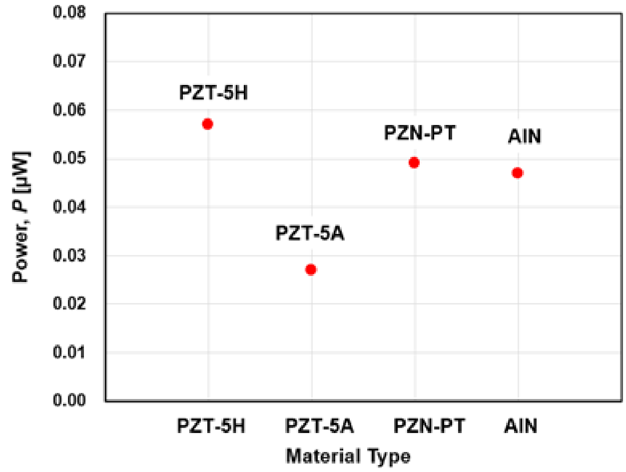

Fig. 8: Generated power as function of the piezoelectric material type of the MEMS device.

3.1. Simulation on NanoHUB

After tweaking the settings, we obtained a peak power of 0.074 μW and a peak voltage of 1.75 mV at 182 Hz, as seen in Fig. 10 and Fig. 11, respectively.

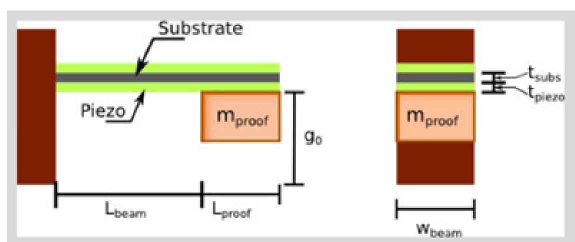

Fig. 9: Piezoelectric beam designed on NanoHUB simulation.

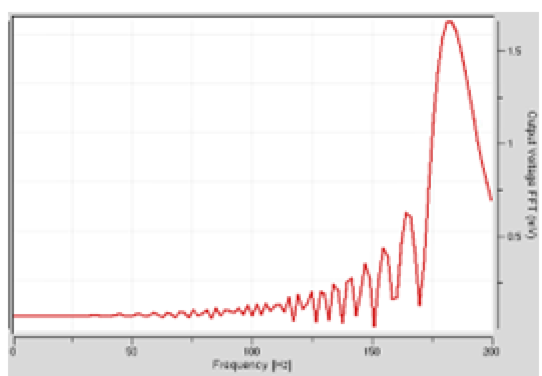

Fig. 10: The voltage generated by the MEMS device as a function of frequency [25].

The output power of the MEMS is depicted in Fig. 12 as a function of load resistance. The output power rises first from 1 to 1000 Ω, then falls as the load resistance rises.

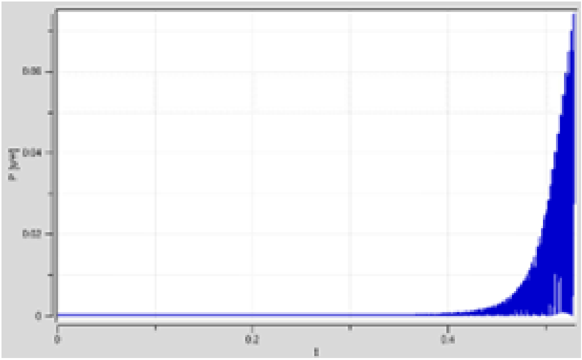

Fig. 11: Generated power with respect to the time [25].

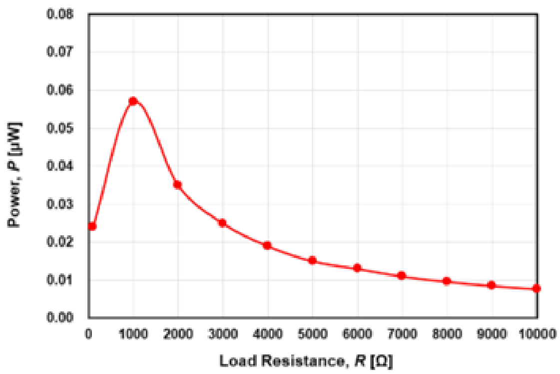

Fig. 12: Generated power as function of the load resistance of the MEMS device.

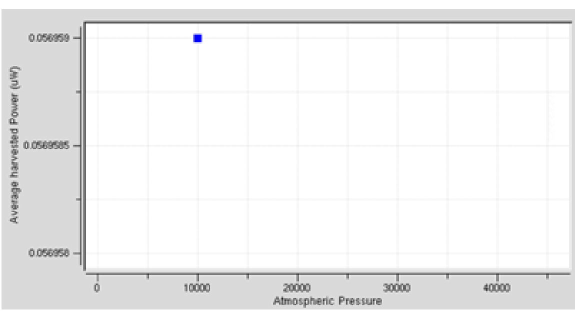

Fig. 13: Generated power measured at atmospheric pressure of 10 KPa.

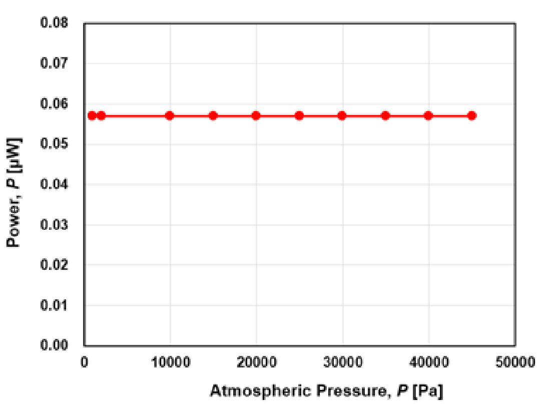

Fig. 14: Generated power as function of the atmospheric pressure of the MEMS device.

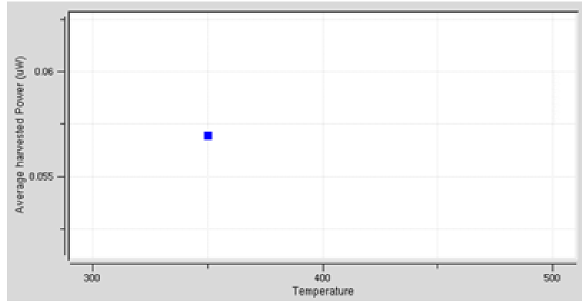

Fig. 15: Generated power measured at temperature of 350K.

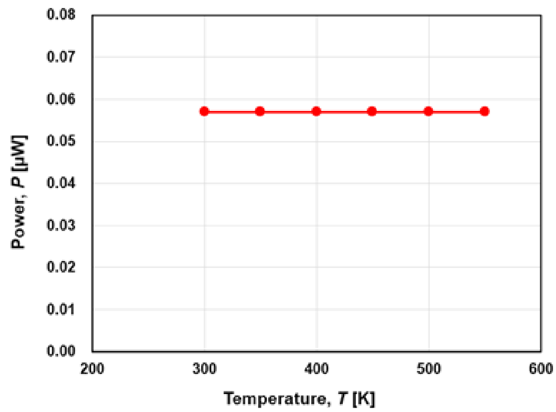

Fig. 16: Generated power as function of the temperature of the MEMS device.

Generated power measured at atmospheric pressure of 10 KPa is shown in Fig. 13. When changing the atmospheric pressure from 1000 Pa to 45 KPa, the harvested energy remains stable and equal to 0.057 μW, as seen in Fig. 14. Generated power measured at a temperature of 350 K is 0.057 μW, as shown in Fig. 15. From Fig. 16, we find that the energy harvested stays constant at 0.057 μW despite the variation in temperature from 300 K to 550 K. These results demonstrate the stability of energy harvesting of the MEMS device when subjected to variations in temperature and environmental pressure.

3.2. Comparison of NanoHUB results and COMSOL results

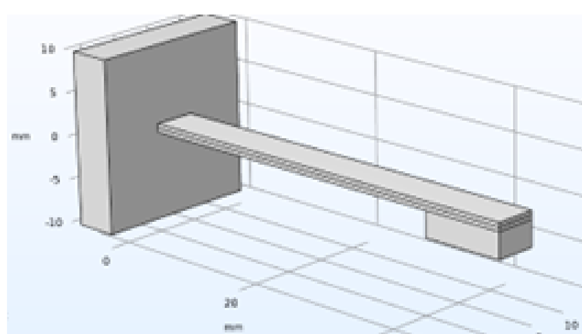

Fig. 17: A piezoelectric beam that was designed using COMSOL simulation [25].

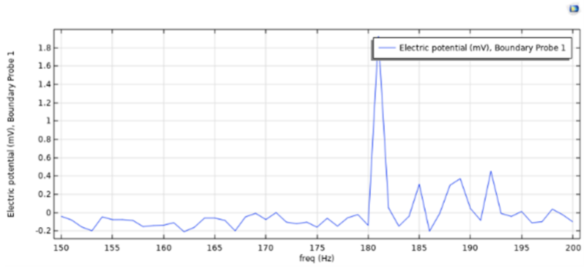

Fig. 18: The electric potential generated as a function of frequency [25].

After optimizing the parameters, we achieved a peak voltage of 1.9 mV at 182 Hz, as seen in Fig. 18. This result agrees well with the simulation result of NanoHUB simulation.

4. Conclusion

Through the use of NanoHUB and COMSOL simulation, we examined the effectiveness of a piezoelectric vibration energy harvester in this work. According to the simulation's results, the MEMS exhibited good performance, including a peak power of 0.074 μW and a peak voltage of 1.9 mV at 182 Hz. Furthermore, the device simulations demonstrated that as the load resistance is raised, the output power first rises before falling. The output voltage of this device can be improved by using the array structure of these devices. We believe that these results could supply power to low- power IoT sensors. This article also demonstrates the stability of energy harvesting of MEMS components when subjected to variations in temperature and environmental pressure.

References

[1] A. Erturk and D. J. Inman, "Piezoelectric Energy Harvesting," *New York: John Wiley & Sons*, 2011.

[2] B. Yang, H. Liu, J. Liu, C. Lee, "Micro and Nano Energy Harvesting Technologies," *Artech House Publishers*, 2014.

[3] J. F. Nye, "Physical Properties of Crystals," *New York: Oxford University Press*, vol. 1990.

[4] IEEE, "IEEE Standard on Piezoelectricity," *ANSI/IEEE Std 176*, 1987.

[5] R. Ghodssi and P. Lin, "MEMS Materials and Process Handbook," *New York: Springer*, 2011.

[6] C. R. Bowen et al., , "Piezoelectric and Ferroelectric Materials and Structures for Energy Harvesting Applications," *Energy Environ. Sci*, vol. 7, pp. 25–44, 2014.

[7] A. Erturk and D. J. Inman, "Piezoelectric Energy Harvesting," *Energ. Convers. Manage*, vol. 50, No. 7, p. 1847–1850, 2009.

[8] S. Roundy and P. K. Wright, "A Piezoelectric Vibration Based Generator for Wireless Electronics," *Smart Mater. Struct*, vol. 13, No. 4, p. 1131–1142, 2004.

[9] S. R. Anton and H. A. Sodano, "A Review of Power Harvesting Using Piezoelectric Materials (2003–2006)," *Smart Mater. Struct*, vol. 16, No. 3, p. R1–R21, 2007.

[10] [Q. M. Wang et al, "Theoretical Analysis of the Sensor Effect of Cantilever Piezoelectric Benders," *J. Appl. Phys*, vol. 85, No. 3, p. 1702–1712, 1999.

[11] B. S. Lee et al, "Piezoelectric MEMS Generators Fabricated with an Aerosol Deposition PZT Thin Film," *J. Micromech. Microeng*, vol. 19, No. 6, p. 065014, 2009.

[12] S. B. Kim et al, "Comparison of MEMS PZT Cantilevers Based on d31 and d33 Modes for Vibration Energy Harvesting," *J. Micorelectromech. S*, vol. 22, No. 1, p. 26– 33, 2013.

[13] W. Beckert and W. S. Kreher, "Modelling Piezoelectric Modules with Interdigitated Electrode Structures," *Comput. Mater. Sci*, vol. 26, p. 36–45, 2003.

[14] C. Bowen et al, "Optimisation of Interdigitated Electrodes for Piezoelectric Actuators and Active Fiber Composites," *J. Electroceram*, vol. 16, No. 4, p. 263–269, 2006.

[15] R. D. Blevins, "Formulas for Natural Frequencies and Mode Shape," *Malabar, FL: Robert E. Krieger Publishing*, 1979.

[16] P. D. Mitcheson et al, "Architectures for Vibration-Driven Micropower Generators," *J. Microelectromech. S*, vol. 13, No. 3, p. 429–440, 2004.

[17] S. J. Roundy, "Energy Scavenging for Wireless Sensor Nodes with a Focus on Vibration to Electricity Conversion," *Ph.D. Thesis, University of California, Berkeley*, 2003.

[18] H. B. Fang et al., "Fabrication and Performance of MEMS-Based Piezoelectric Power Generator for Vibration Energy Harvesting," *Microelectron. J*, vol. 37, No. 11, p. 1280–1284, 2006.

[19] A. Niranjan and P. Gupta, "Modeling and Simulation Software in MEMS Design," *International Journal of Engineering and Advanced Technology (IJEAT)*, vol. 9, No. 3, pp. 2501–2506, 2020.

[20] E. Martínez-Cisneros, L. A. Velosa-Moncada, J. A. D. Angel-Arroyo, L. A. Aguilera-Cortés, C. A. Cerón-Álvarez, A. L. Herrera-May, "Electromechanical Modeling of MEMS-Based Piezoelectric Energy Harvesting Devices for Applications in Domestic Washing Machines," *Energies*, vol. 13, No 3, pp. 617–633, 2020.

[21] Y. Yaowen and T. Lihua, "Equivalent circuit modeling of piezoelectric energy harvesters," *J. of intelligent material systems and structures*, vol. 20, no 18, pp. 2223–2235, 2009.

[22] S. Kundu and H. B. Nemade, "Modeling and Simulation of a Piezoelectric Vibration Energy Harvester," *Procedia Engineering*, 2016.

[23] L. Jing-Feng, "Fundamentals of Piezoelectricity," *Wiley-VCH GmbH*, 2021.

[24] H. B. Fang et al., "Fabrication and Performance of MEMS-Based Piezoelectric Power Generator for Vibration Energy Harvesting," *Microelectron. J*, vol. 37, 11, p. 1280–1284, 2006.

[25] Dao Ngoc Tuan et al., "Modeling and Simulation of MEMS-Based Piezoelectric Energy Harvester," *Pro. 2022 International Conference on IC Design and Technology (ICICDT)*, pp. 21–23, 2022.

Tuan Ngoc Dao is currently undergraduate student at The University of Danang - Vietnam Korea University of Information and Communication Technology (VKU). His research interests include electronics and the physics of semiconductors.

Phuoc Thanh Quang Le is currently undergraduate student at The University of Danang - Vietnam Korea University of Information and Communication Technology (VKU). His research interests include electronics and the physics of semiconductors.

Tho Quang Than received B.Sci. degree in engineering from The University of Danang - University of Science and Technology (DUT), Danang, Vietnam in 2006. He is currently engineer at Central Power Corporation (EVNCPC), Danang, Vietnam. His research interests include solar cell, Energy Harvesting, and power electronics.

Son Thanh Nguyen received a Bachelor degree from Danang University of Science and Technology, Master and Doctor degrees from Nagaoka University of Technology. Currently he is a Junior Associate Professor at National Institute of Technology, Kushiro College, Japan. His research focuses on advanced composites with self-healing ability; tailoring nanostructured materials by electric field; electronic and magnetic materials; and 3D-nano printing technology.

Thanh Tung Huynh received his B.Sci and M.Sci in Japan and Ph.D. in Australia. He is currently a lecturer at the Faculty of Electronics and Telecommunication, University of Science and Technology (DUT), The University of Danang. His research interests include electronics and the physics of semiconductors.

Phuoc-Anh Le received a Bachelor degree and Master degree from Vietnam National University-Hanoi, and PhD degree from National Yang Ming Chiao Tung University, Hsinchu, Taiwan in 2021. He worked for Faculty of Textile Science and Technology, Shinshu University, Japan until 2022. Currently he works as a researcher at VNU Vietnam Japan Universty. His research focuses on Functional Materials for Sustainable Energy Applications.

Phuc Hong Than received B.Sci., M.Sci., and Ph.D. degree in engineering from the University of Electro – Communications, Tokyo, Japan, in 2011, 2013, and 2016, respectively. From 2016 to 2017, she was a device physicist at Fuji Electric Corporation in Matsumoto, Japan. In 2018, she joined the National Institute of Information and Communications Technology (NICT), Japan. Her research activities were in heteroepitaxial growth and characterization of compound semiconductors and development of Si VLSI technologies and devices. She joined Duy Tan University (DTU) in 2020 and is currently lecturer at DTU. Her present research interests include process technology and device design of semiconductor devices in Si, SiC and GaN, such as SBD, BJT, MOSFET, and IGBT.

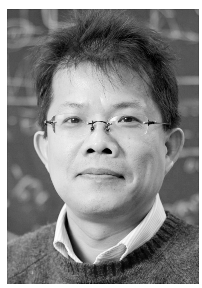

Cong-Kha Pham received the B.S., M.S., and Ph.D. degrees in electronics engineering from Sophia University, Tokyo, Japan. He is currently a Professor with the Department of Information and Network Engineering, The University of Electro-Communications (UEC), Tokyo. His research interest includes the design of analog and digital systems using integrated circuits.